Springer

KSME

Journal of Mechanical Science and Technology 25 (6) (2011) 1449~1456
www.springerlink.com/content/1738-494x
DOI 10.1007/s12206-011-0429-5

Experimental hover performance evaluation on a small-scale rotor using a rotor test stand †

Byoung-Eon Lee, Young-Seop Byun, Jeong Kim and Beom-Soo Kang*

Department of Aerospace Engineering, Pusan National University, Busan, 609-735, Korea

(Manuscript Received November 9, 2009; Revised December 14, 2010; Accepted March 15, 2011)

Abstract

This paper presents the work being carried out in order to deduce hover performance of a small-scale single rotor blade as a preliminary study of a small coaxial rotor helicopter development. As an initial research, a test stand capable of measuring thrust and torque of a small-scale rotor blade in hover state was constructed and fabricated. The test stand consists of three parts; a rotating device, a load measuring sensor and a data acquisition system. Thrust and torque were measured with varying collective pitch angle at fixed RPM. Through this research, hover performance tests were conducted for a small-scale single rotor blade operating in low Reynolds numbers ($Re \approx 3 \times 10^5$). The rotor blades investigated in this paper have maximum FM values varying from 0.59 to 0.65, which are low relative to modern full-scale helicopters. From these differences in FM between a small and a full-scale helicopter, the induced power factor is determined as varying from 1.35 to 1.42. Through this study, tests of hover performance were conducted for a single small-scale rotor blade, as well as verifying the test stand itself for the acquisition of hover performance.

Keywords: Hover performance; Rotor test stand; Small-scale rotor blade; Induced power factor

1. Introduction

With the diversification of applications of Unmanned Aerial Vehicles (UAVs), many studies and developmental efforts are underway for UAVs for various civil purposes. Research and development are increasing for rotary wing UAVs such as helicopters, for simple aerial surveillance and observation that arise from their hovering capabilities and slow flight [1]. Our goal is the development of a coaxial helicopter that has the advantage of a higher gross take-off weight than single-rotor helicopters, and we are investigating the feasibility of a small coaxial unmanned helicopter for a UAV that performs close-range surveillance [2]. Recently, an actual flight test was completed through the design and fabrication of a small coaxial unmanned helicopter, as shown in Fig. 1 [3].

Fig. 1. Configuration of a coaxial helicopter.

The preliminary design of a helicopter configuration is accomplished through iterative computations that entail a compromise between various design factors so that the appropriate configuration can be derived to achieve the stated mission. The prediction of the performance of the rotor blades is especially important for determining design factors such as weight and size of the helicopter. Generally, the prediction of helicopter performance refers to the estimation of the power that is required for a given flight condition. However, in the development of small-scale helicopter vehicles, it is difficult to predict the required power through the methods used for full-scale helicopters, because the small-scale helicopter has different characteristic such as blade tip speed, geometry and size.

In most cases, the prediction of the power requirement in a preliminary design is conducted through a modified momentum theory. As shown in Eq. (1), the power required to hover

† This paper was recommended for publication in revised form by Associate Editor Do Hyung Lee

* Corresponding author. Tel.: +82 51 510 2310, Fax.: +82 51 513 3760
E-mail address: bskang@pusan.ac.kr

has two main components, induced and profile power. Induced power is related to the generation of the thrust, and it also includes losses caused by physical phenomena ignored in the assumptions made in momentum theory. Profile power includes all the viscous effects that influence the blade's performance.

$$P = \frac{\kappa T^{3/2}}{\sqrt{2\rho A}} + \rho A(\Omega R)^3 \left(\frac{\sigma C_{do}}{8}\right) \quad (1)$$

The momentum theory has an error of about 20% in most cases. These errors between the momentum theory and actual phenomena occur because viscous effect has been ignored [4]. Especially, when Reynolds number is low, the higher viscosity effect leads to this increased discrepancy. Therefore, to apply the theories to an actual design, corrections are required with regard to the induced power factor and the average profile drag coefficient, which varies with the flight condition. In particular, induced power must be corrected for a number of non-ideal, but real, physical effects, such as non-uniform inflow, tip losses, wake swirl, imperfect wake contraction and a finite number of blades, by multiplying by the induced power factor. The induced power factor must be empirically determined for each rotor. For this reason, most helicopter manufacturers use their own measurements and experience in preliminary designs to estimate the values of the induced power factor [4]. However, it is difficult to predict and analyze the required power of a small-scale helicopter because of the lack of test data for small-scale rotor blades that operate at a low Reynolds numbers ($\mathrm{Re} \approx 3 \times 10^5$).

In addition, the wakes on the upper and lower rotors of a coaxial helicopter interact with one another to produce a more complicated flow field. A NASA report that gives a broad perspective of the aerodynamic issues and state of the art of coaxial helicopter technology was published by Coleman [5]. It gives a good summary of coaxial rotor designs along with a comprehensive list of relevant citations on performance, wake characteristics and proposed methods of performance analysis. However, there has been insufficient research on small-scale coaxial helicopters to date. Further, data for understanding the characteristics of coaxial rotor configurations, e.g., mutual interference effects and interference caused by the wakes, are very rare. For these reasons, to predict the power requirements of coaxial rotors, a correction is required with regard to the interference-induced power factor, including the induced power factor of each rotor blade, as per Eq. (2) [6].

$$P = \frac{\kappa\kappa_{\mathrm{int}}(2T)^{3/2}}{\sqrt{2\rho A}} + \rho A(\Omega R)^3 \left(\frac{2\sigma C_{do}}{8}\right) \quad (2)$$

Therefore, after the performance characteristics of each rotor blade are confirmed, one should conduct experiments and undertake analysis of the interference effects of coaxial rotors to predict the required power. In particular, it is necessary to test and verify the aerodynamic performance of the small-scale rotor blades to be used in coaxial helicopters because aerodynamic data and experimental results are currently unavailable.

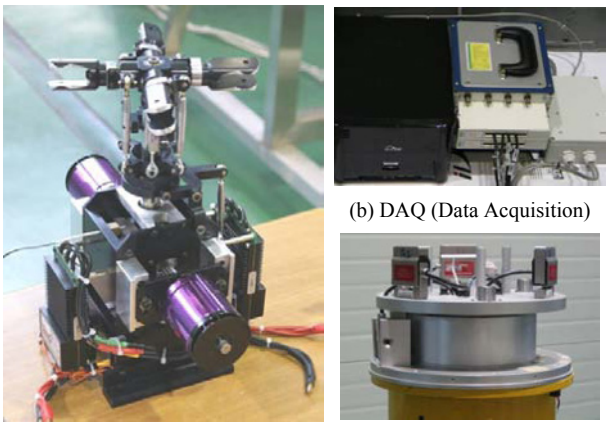

(a) Rotating Device (b) DAQ (Data Acquisition) (c) Load Measuring Sensor

Fig. 2. Components of test equipment.

Accordingly, we have conducted research employing a rotor test stand for single and multiple rotor blades to measure the hover performance of a small-scale rotor blade. Hence, this paper presents research that is being carried out to deduce the hover performance of a single rotor blade; the study is preliminary to the development of a small coaxial rotor helicopter. For this preliminary study, a rotor test stand that is capable of measuring the thrust and torque of a small-scale rotor blade in a hover state was constructed and fabricated. The rotor test stand consists of a rotating device, a load-measuring sensor, and a data acquisition system. The thrust and torque are measured for varying collective pitch angles at fixed rotational speeds. The resulting data are transferred to and monitored on the acquisition system. Through this research, hover performance tests were conducted for a single small-scale rotor blade that operated at low Reynolds numbers ($\mathrm{Re} \approx 3 \times 10^5$); we also were able to verify that the rotor test stand was a suitable tool for the acquisition of hover performance.

2. Construction of and experiments with the rotor test stand

2.1 Construction of the rotor test stand

The rotor test stand was constructed to measure the thrust and torque of a small rotor in the hover state. It consists of the rotating device, instrumentation for sensors, and a data acquisition system, as shown in Fig. 2.

The rotating device is composed of a rotor hub and a power transmission, as shown in Fig. 3. The rotor hub is four-bladed ('A' in Fig. 3) and of the semi-articulated type with a flap hinge. The power transmission equipment consists of a 2 KW BLDC (BrushLess Direct Current) motor ('B' in Fig. 3) with a

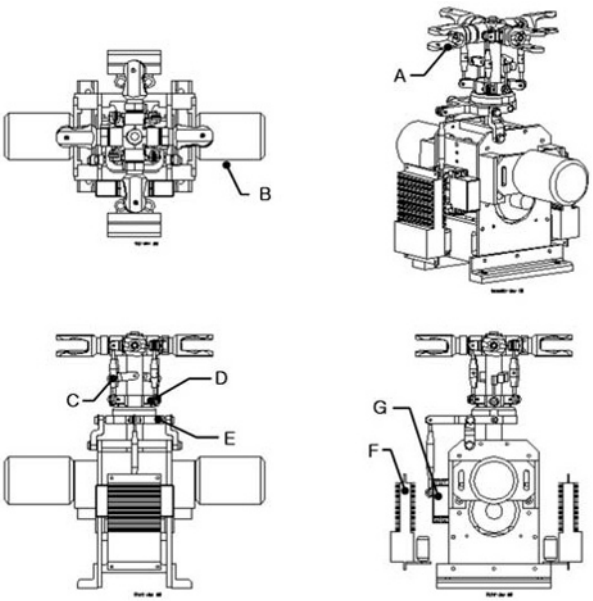

- A: Semi-articulated Hub.
- B: Driving Motors (2EA).
- C: Collective Pitch Link (4EA).
- D: Swash-Plate (Rotary).
- E: Swash-Plate (Stationary).
- F: ESC (Electronic Speed Controller) (2EA).
- G: Servo Actuator (2EA).

Fig. 3. Rotor hub and driving device.

5.4:1 gear reduction ratio, and the electric power was supplied through a 5 KW rectifier.

To measure the performance of small-scale rotor blades experimentally, thrust and power are required to validate rotor performance. Hence, three physical quantities must be measured by the rotor test stand: thrust, torque and rotational speed.

A National Instruments DAQ card and a SC-2345 carrier box with NI SCXI-1000, 1120D, 1600 and NI SCC modules were used for signal conditioning and data acquisition, and the software used was LabView 7.0. Sensors were installed to capture the thrust and torque that act on the hub shaft as the hub rotates. The load limits are 1.47 kN and 45.6 Nm for the thrust and torque, respectively. Thrust is measured by three load cells and torque is measured by one load cell. In addition, the instrumentation includes photo sensors for measuring the rotational speed, sensors for measuring the voltage and current, and a 3-axis accelerometer for measuring the vibration of the rotor test stand post. The data that are measured by each sen-sor are confirmed and gathered at a control PC through the data acquisition system in real time, as shown in Fig. 4. The rotational speed and the collective pitch angle of the rotors are controlled by the control PC through an Electronic Speed Controller (ESC; 'F' in Fig. 3), a servomotor, and a servo actuator ('G' in Fig. 3).

Tests of the hover performance of the rotor blade were performed in a way that minimized the ground effect and confirmed the reliability of the experiments at a test station in the Korea Aerospace Research Institute. The rotor test stand was

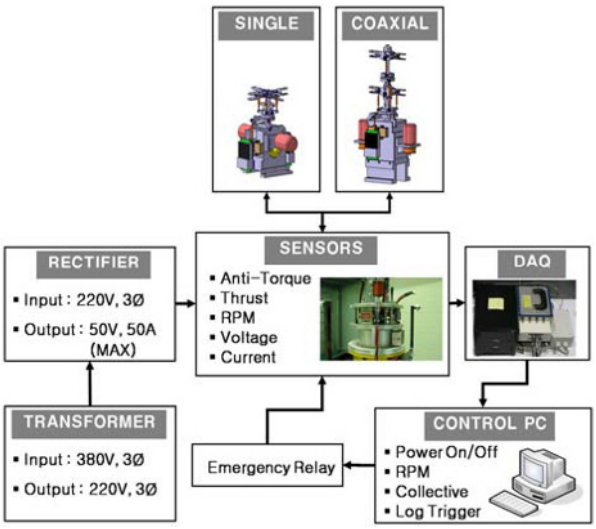

Fig. 4. Organization of rotor test stand.

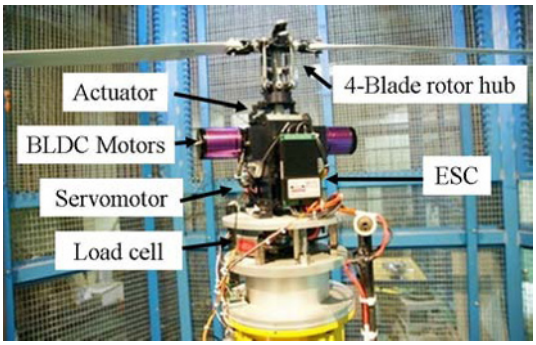

Fig. 5. Rotor hub model mounted for the test.

constructed and integrated with the various components, as shown in Fig. 5. The test station that was arranged for the buildup and experimental testing of a rotor system two meters in diameter features a steel chain link fence around the walls to curtail wall effects [7]. In accordance with various experimental studies [8] in which the distance of the rotor from the ground plane was varied, the ground effect was found to be negligible when the distance from the ground plane to the rotor was more than 2.5 times the radius of the rotor blade. The rotating device was therefore located 2.9 meters above the ground plane, to accommodate the rotor blades used in this research. In this manner, the reliability of the measured test data was ensured, given the absence of ground and wall ef-fects, which are induced by the wake from the revolving rotor blade.

2.2 Calibration of the rotor test stand

Although the test equipment was constructed using the sensors and other equipment described, errors in data acquisition in an actual hover test can occur because of discrepancies in the output values generated from each component. To solve this problem and to confirm the accuracy of the test equipment, a calibration test was performed using the sensors of the con-

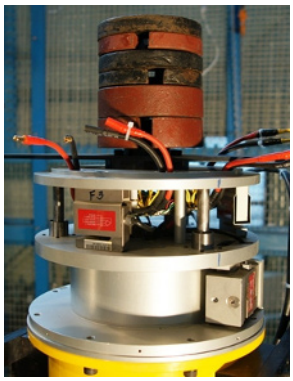

(a) Thrust

(b) Torque

Fig. 6. Calibration using a balance weight.

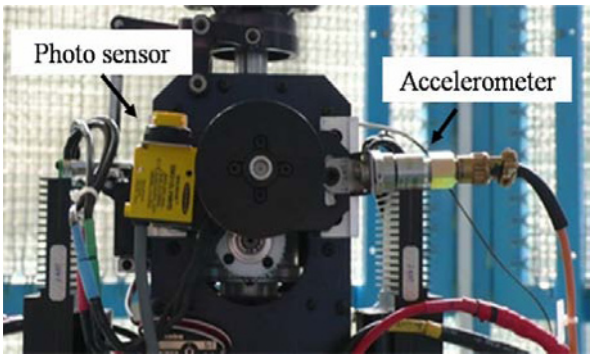

Fig. 7. Calibration of tracking and balancing.

structed test equipment [9]. The calibration test compared the applied and expected loads using the hysteresis curve.

To apply the load, we used a balance weight, as shown in Fig. 6. The errors that were generated for thrust and torque calibration were 0.27% and 0.17%, respectively. The calibration test for the electric current and voltage was performed by comparing the applied and expected outputs using an electric power analyzer.

Additionally, tracking and balancing tests were performed to minimize the vibration of rotor blade. Fig. 7 shows a photo sensor and an accelerometer used in the tracking and balancing tests. Calibrating progress includes static balancing, tracking and dynamic balancing test, resultantly improved static and dynamic balance.

In any experimental setup with high speed rotating equipment, it should be checked for vibration to avoid disastrous accidents from resonance. In this test, to capture the vibration characteristics of the post of the rotor test stand, FFT (Fast Fourier Transform) analysis was conducted after calibration tests of each component. The resonance frequency of the rotor test stand post was 16Hz (about 1,000RPM), as shown in Fig. 8. This RPM was avoided or passed quickly as soon as possible during a rotational test.

2.3 Results of the tests

After the reliability of the rotor test stand had been verified through the above calibration tests, a rotor blade suitable for unmanned coaxial-rotor helicopters was mounted on the rotating device and then a rotor test was conducted to evaluate the hover performance. In this manner, the verification of the test stand was accomplished. The rotor-blade sets used in this investigation are commercial products crafted from composite material. They had smooth skins and untwisted, rectangular platforms with a NACA 0015 section, as shown in Fig. 9 and Table 1. To acquire various kinds of hover performance, four different types of rotor blade were used.

The hover performance tests were conducted for various collective pitch angles while the rotational speed was fixed. The collective pitch angle of the blades was manually set on

Table 1. Specifications of the rotor blades.

Parameter	Unit	Specification			
Airfoil	N/A	NACA 0015			
Diameter	mm	1260	1400	1580	1620
Weight	g	108	113	234	180
Root-cut	mm	170 (0.270R)	170 (0.243R)	205 (0.263R)	205 (0.253R)
Chord length	mm	50	50	59	59
Aspect ratio	N/A	10.6	12	11.7	12
Twist angle	deg	0	0	0	0
Taper	N/A	1	1	1	1
Solidity	N/A	0.0505	0.0455	0.0475	0.0464

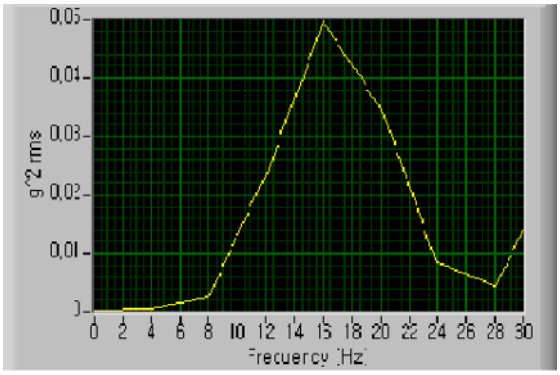

Fig. 8. FFT analysis of rotor test stand.

Fig. 9. Shape of rotor blade.

Fig. 10. Correction of collective pitch angle.

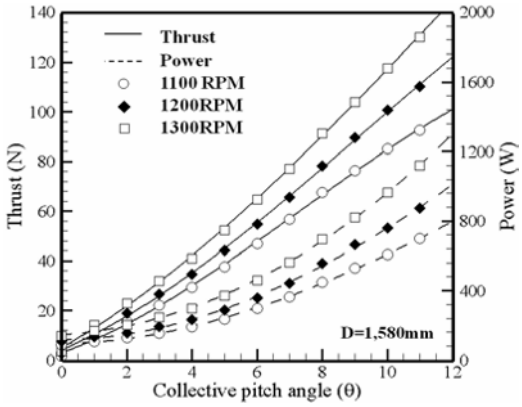

Fig. 11. θ vs. thrust and power.

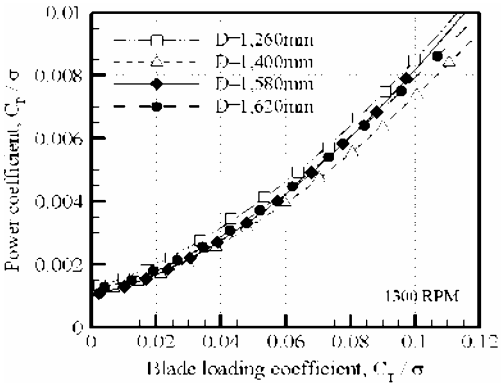

Fig. 12. C_T/σ vs. C_P/σ for same rotational speed (1,300 RPM).

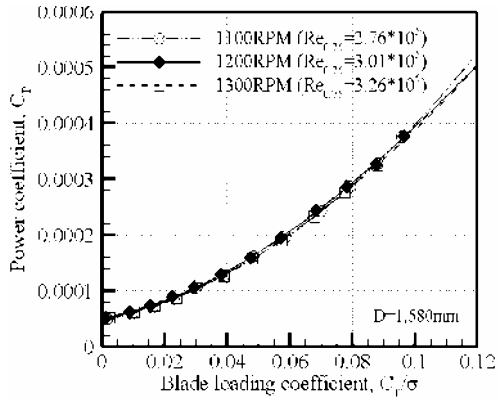

Fig. 13. C_T/σ vs. C_P/σ for same diameter (1,580mm).

the rotor grips using a commercial protractor that provides 0.1° precision, as shown Fig. 10. After a collective pitch angle was set, the rotor balance and blade tracking were checked. Then the rotational speeds for each rotor were set from 1100 RPM to 1300 RPM in steps of 100 RPM, and the collective pitch angles were varied from 0° to 11° in steps of 1° while the rotational speeds were fixed. The thrust and torque were measured at each collective pitch angle for 10 seconds and the measured data were transmitted to the control PC. Tests were performed for increasing collective pitch angles at fixed rotational speeds. To confirm the repeatability of the test results, the tests were performed three times.

The thrust and the torque were measured for various collective pitch angles at 1100, 1200 and 1300 RPM. Fig. 11 is the result with the rotor blade of 1580mm diameter correlated by the thrust and the power for various collective pitch angles.

Fig. 12 shows the test results for the blade-loading coefficient vs. the power coefficient at 1300 RPM for each rotor blade. Although the rotor blade with 1,580mm diameter (C) and 1,620mm diameter (D) have similar tendency since they have similar planform, the rotor blade with 1,400mm diameter (B) distinctively shows better performance than the rotor blade with 1,260mm diameter (A) due to smaller root-cut ratio, which decreases solidity and increases aspect ratio, in contrast to the fact that (B) has longer length than (A) as shown in Table 1.

As shown in Fig. 13, for a given diameter, a stable result was acquired irrespective of the rotor speed, because the rotor test stand was supplied with sufficient power by the rectifier. Using the test results, the power requirements of a single rotor blade were acquired for each collective pitch angle and the aerodynamic characteristics of each rotor blade can be deduced from the results.

2.4 Hover performance of the rotor blade

Generally, to illustrate the hovering efficiency, a figure of merit (FM) is used. The FM is a standard non-dimensional measure of the hovering thrust efficiency and is defined as the ratio of the ideal power that is required for hovering to the actual power required. That is,

$$FM = \frac{Ideal\ \ power\ required\ \ to\ hover}{Actual\ \ power\ required\ \ to\ hover} < 1. \quad (2)$$

In actual power measurements, a viscous effect affects both the induced power and the profile power. The FM is expressed in Eq. (3) from simple momentum theory. It can be used as a gauge of the efficiency of a given hovering rotor in terms of generating thrust for a given power.

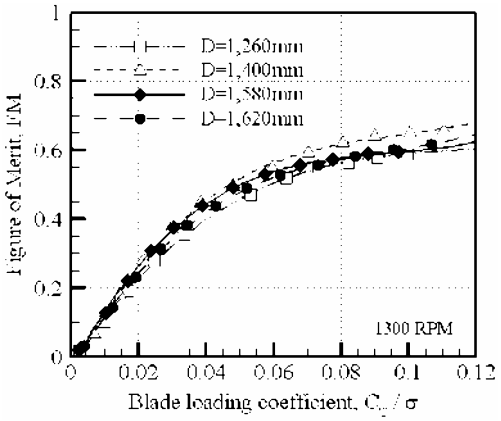

Fig. 14. Variation of C_T/σ with FM for different rotor blade.

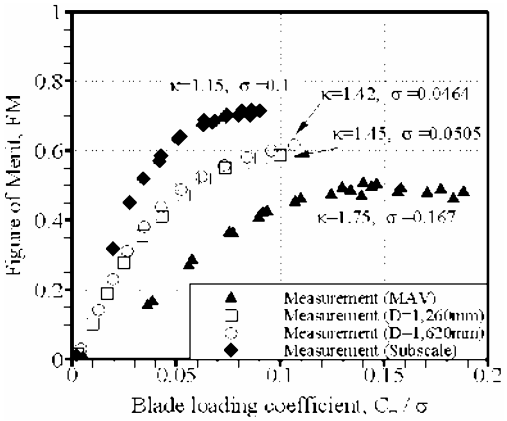

Fig. 15. Measured FM for diverse rotor blade [4].

$$FM = \frac{P_{ideal}}{P_{meas}} = \frac{C_{T,meas}^{3/2}/\sqrt{2}}{C_{P,meas}} = \frac{C_{T,meas}^{3/2}}{\sqrt{2}\,C_{P,meas}} \tag{3}$$

In this research, FM is calculated as a function of the measured thrust coefficient and the power coefficient. As shown in Fig. 14, the rotor blades investigated in this paper have maximum FM values varying from 0.59 to 0.65, although modern full-scale helicopters can have maximum FM values of the order of 0.8. To comprehend the difference in FM between a small and a full-scale helicopter, a modified momentum theory is applied, as shown in Eq. (3). The induced power factor that is unique to a rotor blade is deduced from the appli-cation of Eq. (3) to the measured relationship between the thrust coefficient and the power coefficient. After Eq. (3) is approximated by a linear equation through a least-squares approach, the induced power factor is calculated as the slope of the linear fit, and the profile drag coefficient is calculated as the intercept (on the y-axis) of the linear fit. As a result, the induced power factor is calculated to vary from 1.35 to 1.42, which is more than that for a full-scale helicopter, of the order of 1.15, and lower than that for a Micro Aerial Vehicle (MAV), viz., 1.75, as obtained through experimentation in Ref. [10].

With small-scale rotor blades that operate at low Reynolds numbers, the inner section of the blade makes little contribution to the lift. For this reason, as the span-wise distribution of the lift is inclined towards the blade tip, the induced power is estimated to increase relatively. Fig. 15 reveals a comparison of the results deduced from the experiments in this study and existing experimental data on a subscale helicopter and an MAV.

Eq. (3) can also be expressed as Eq. (4), whereby the induced power factor is applied using a non-ideal approach.

$$FM = \frac{P_{ideal}}{\kappa P_{ideal} + P_o} = \frac{\frac{C_T^{3/2}}{\sqrt{2}}}{\frac{\kappa C_T^{3/2}}{\sqrt{2}} + \frac{\sigma C_{do}}{8}} \tag{4}$$

From the definition of Eq. (4), it is apparent that the FM of a small-scale rotor blade has a low value because the induced power factor is increased.

As discussed above, we figure out the FM of a small-scale rotor blade through the empirical relationship between the thrust coefficient and the power coefficient. Additionally, for verifying this result, an existing-developed an unsteady panel code coupled with a time-marching free wake model that applied field velocity approach is used. A number of panels are applied for each blade: 24 panels in the chord-wise direction and 20 panels with span-wise direction. An analysis is performed wherein the collective pitch angle of the blade is set at $2^\circ, 4^\circ, 6^\circ, 8^\circ, 10^\circ$ and 12°, and the thrust coefficient converges after 16 revolutions of the blade. Fig. 16 shows the result of the comparison between two kinds of blade; they are in good agreement with the FM that varies with the blade loading coefficient.

3. Conclusion

This paper presents work that is being carried out to deduce the hover performance of a single small-scale rotor blade that operates at a low Reynolds number ($Re \approx 3 \times 10^5$), as a preliminary study for the development of a small coaxial-rotor helicopter. As an initial step in the research, a rotor test stand that was capable of measuring the thrust and torque of a small-scale rotor blade in the hover state was constructed and fabricated, to measure the performance of small-scale rotors experimentally. Tests were performed at increasing collective pitch angles and fixed rotational speeds for each rotor blade. The experimental results presented show that a stable result is acquired irrespective of the rotor speed for a given diameter. Using the test results, the power requirements of a single rotor blade are acquired at each collective pitch angle and the aerodynamic characteristics of each rotor blade can be deduced. The rotor blades investigated in this paper have maximum FM values varying from 0.59 to 0.65, which are low relative to modern full-scale helicopters that have maximum FM values of the order of 0.8. From these differences in FM between a small- and a full-scale helicopter, the induced power factor is

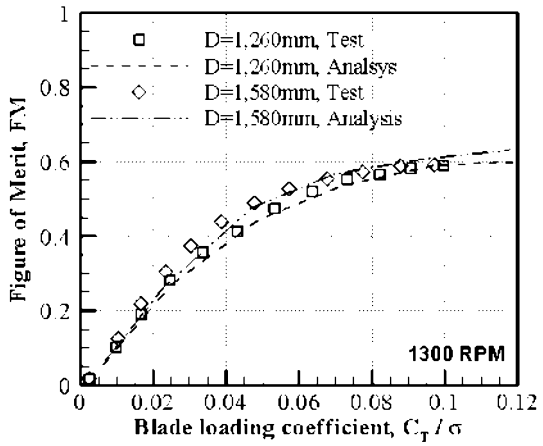

Fig. 16. Comparison with test and analysis result.

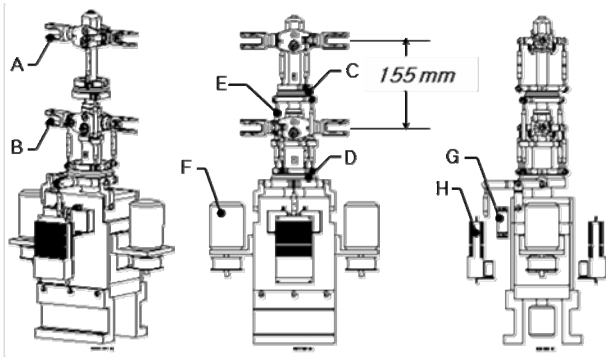

- A: Upper Hub-Rigid Teetering.
- B: Lower Hub-Rigid Teetering.
- C: Upper Swash-Plate.
- D: Lower Swash-Plate.
- E: Inter-Link.
- F: Driving Motor (2EA).
- G: Servo Actuator (2EA).
- H: ESC (Electronic Speed Controller) (2EA).

Fig. 17. Rotor hub of coaxial helicopter.

determined as varying from 1.35 to 1.42. Through this study, tests of hover performance were conducted for a single small-scale rotor blade, as well as verifying the test stand itself for the acquisition of hover performance.

At present, we are building the rotor hub for a coaxial helicopter, as shown in Fig. 17, to achieve the ultimate goal, namely, the acquisition of the hover performance of small-scale coaxial rotor blades. Research is also envisaged for the acquisition of performance data for a multiple blade rotor, i.e., experiments will be performed to determine the hover performance of a four-bladed rotor using the rotor test stand utilized in this research.

Acknowledgment

This work was supported by the Korea Science and Engineering Foundation (KOSEF) NRL Program grant funded by the Korea government (MEST) (ROA-2008-000-10204-0), and this research was financially supported by the Ministry of Education, Science Technology (MEST) and Korea Industrial Technology Foundation (KOTEF) through the Human Resource Training Project for Regional Innovation, Korea government.

Nomenclature

A	: Rotor disk area
c	: Blade chord length
C_{d0}	: Zero lift (average profile) drag coefficient
C_T	: Thrust coefficient
$C_{T,meas}$	: Measured thrust coefficient
C_P	: Power coefficient
$C_{P,meas}$	: Measured power coefficient
FM	: Figure of merit
R	: Rotor blade radius
T	: Rotor thrust
P	: Rotor power
P_{ideal}	: Rotor ideal power
P_{meas}	: Rotor measured power
P_o	: Rotor profile power
κ	: Induced power factor
κ_{int}	: Induced power interference factor
ρ	: Flow density
σ	: Rotor solidity
Ω	: Rotational speed of the rotor

References

[1] K. T. Lee and C. J. Oh, Introduction to mission requirement and technical trend of rotary-wing unmanned aerial vehicle system, *Journal of The Korean Society for Aeronautical and Space Sciences(in Korean)*, 30 (8) (2002) 156-163.

[2] Y. S. Byun, B. E. Lee, J. B. Song and J. Kim, B. S. Kang, Preliminary design of small coaxial unmanned aerial vehicle, *Proc. of KSAS-JSASSS Joint International Symposium* (2006) 29-36.

[3] S. D. Kim, Y. S. Byun, B. E. Lee, J. B. Song and J. Kim, B. S. Kang, Design and fabrication of a small coaxial rotorcraft UAV, *Journal of The Korean Society for Aeronautical and Space Science(in Korean)*, 37 (3) (2009) 29-36.

[4] J. Gordon Leishman, *Principles of helicopter aerodynamics*, second ed, Cambridge Press, USA (2006).

[5] C. P. Coleman, A survey of theoretical and experimental coaxial rotor aerodynamic research, *Proc. of the 19th European Rotorcraft Forum*, Cernobbio, Italy (1993) 14-16.

[6] J. G. Leishman and S. Ananthan, Aerodynamic optimization of a coaxial proprotor, *62th Annual Forum and Technology Display of the American Helicopter Society International*, Phoenix, AZ, May (2006).

[7] J. Joo, J. H. Kim and D. K. Kim, The study on the small-scaled rotor system testing technology using KARI GSRTS, *Proc. of KSAS Fall Conference* (2000) 79-82.

[8] W. Rhee, J. S. Choi, Development of a helicopter rotor test

rig and measurement of aeroacoustic characteristics, *Journal of The Korean Society for Aeronautical and Space Science (in Korean)*, 32 (3) (2004) 10-16.

Byoung-Eon Lee received his B.S. degree in Aerospace Engineering from Pusan National University in 2006, and finished a Ph.D course of study in 2010. He is currently a research engineer of Aerospace Engineering at Pusan National University in Busan, Korea. His research interests include helicopter rotor blade, coaxial helicopter and unmanned aerial vehicle.

Beom-Soo Kang received his B.S. degree in Mechanical Engineering from Pusan National University in 1981, and his M.S. degree in Aerospace Engineering from KAIST in 1983 in Korea. He then obtained his Ph.D. degree from the University of California at Berkeley, USA, in 1990. Dr. Kang is currently a Professor at the Department of Aerospace Engineering at Pusan National University in Busan, Korea. His research interests include coaxial helicopter and Unmanned Aerial Vehicle.